energies

Article

Improved Voltage Flux-Weakening Strategy of Permanent Magnet Synchronous Motor in High-Speed Operation

Hyun-Jae Lee and Jin-Geun Shon *

Department of Electrical Engineering, Gachon University, Seongnam-Si 13120, Korea; lhj501@gachon.ac.kr
* Correspondence: shon@gachon.ac.kr

Abstract: This paper presents an improved voltage flux-weakening strategy of a permanent magnet synchronous motor (PMSM) in a high-speed operation. The speed control performance using voltage flux-weakening control is not affected by the motor parameters, so it is used in various motors for high-speed operations. In general, the voltage flux-weakening control uses voltage references to generate a flux axis current reference. However, there may be errors between the voltage reference and the actual voltage flowing into the motor. This causes an error in the current reference generation and reduces the efficiency of the inverter and motor due to the use of more current. In this paper, the problems that can occur due to voltage errors were analyzed through theoretical approaches and simulations, and improved voltage flux-weakening control to resolve these problems was presented. This method's advantage is that the error between the voltage reference and the voltage applied to the motor can be minimized, and the target speed can be reached with minimum current. As a result, it was possible to increase the energy efficiency by reducing the amount of current flowing through the motor. The effect of the improved voltage-based flux-weakening control method was verified through simulations and experiments. As a result, the voltage errors were reduced by approximately 2.16% compared to the general method. Moreover, the current used in the field-weakening control region was reduced by up to 27.17% under the same torque condition.

Keywords: flux-weakening control; high-speed operation; permanent magnet synchronous motor (PMSM); voltage closed-loop control

check for updates

Citation: Lee, H.-J.; Shon, J.-G. Improved Voltage Flux-Weakening Strategy of Permanent Magnet Synchronous Motor in High-Speed Operation. *Energies* **2021**, *14*, 7464. https://doi.org/10.3390/en14227464

Academic Editor: Federico Barrero

Received: 20 October 2021
Accepted: 5 November 2021
Published: 9 November 2021

Publisher's Note: MDPI stays neutral with regard to jurisdictional claims in published maps and institutional affiliations.

Copyright: © 2021 by the authors. Licensee MDPI, Basel, Switzerland. This article is an open access article distributed under the terms and conditions of the Creative Commons Attribution (CC BY) license (https://creativecommons.org/licenses/by/4.0/).

1. Introduction

Various policies are being established worldwide for sustainable production and consumption of energy to minimize the detrimental effects of fossil fuels; this involves reducing carbon emissions and using green energy [1,2]. In particular, machines propelled using fossil fuels, such as automobiles, railways, and ships are being replaced by electrical motors to solve the problem of environmental pollution [3–7].

Various motors are used in such propulsion systems, depending on their purpose or capacity, such as induction motor synchronous motor, and brushless DC motors. Recently, various studies have been conducted using permanent magnet synchronous motors (PMSMs), which have the advantages of high efficiency, high power density, and high reliability compared to other motors [8–12].

Motors used in propulsion systems must perform high-speed operations above the rated speed when necessary [13,14]. In the case of PMSMs, flux-weakening control, which reduces the magnitude of the effective magnetic flux in the air gap by generating a new magnetic flux in the direction opposite to that of the existing magnetic flux, is used to enable high-speed operation [15–18]. Various studies have been conducted on the high-speed operation of motors. In the early days, a method was used to reduce the magnetic flux component current in inverse proportion to the rotor speed [19]. However, this method has a disadvantage in that the surplus voltage required for vector control is not enough. Accordingly, vector control might be inaccurate, leading to difficulty in driving the motor.

To overcome these shortcomings and perform accurate motor speed control, an optimal current control method using voltage limiting conditions and current limiting conditions has been proposed [20,21]. This method expresses the maximum magnitude of voltage that can be applied to the motor and the maximum magnitude of current that can flow into the motor as circles. It determines the most appropriate current point to drive the motor to control the speed, thereby enabling the user to sufficiently obtain the output torque ability of the motor. In addition, a method of controlling the motor by conducting various experiments on the motor and making the characteristics of the lookup table was used [22–24]. However, it has shortcomings in that it requires accurate information on parameters because it is sensitive to changes in motor parameters, and the control design is complicated because the variation characteristics of magnetizing inductance should be considered. To address these problems, various control methods that are less affected by the motor parameters using voltage feedback have been studied [25,26]. Among them, the voltage flux-weakening control was studied for controlling the flux [27,28]. This method carries out flux-weakening control using the magnitude of the voltage applied to the motor. It has advantages in that it is robust against change factors because it does not use motor parameters and the control design is simple. However, owing to motor control characteristics, the indirect voltage-based flux-weakening control method is mainly used. This method does not directly measure the voltage applied to the motor but indirectly calculates the voltage using the output of PI controller [29]. The disadvantage of this method is that the speed control may not be precise if an error occurs between the predicted magnitude of voltage and the actual voltage applied to the motor.

Accordingly, in this study, we considered the possibility that an error may occur between the previously used voltage command and the voltage flowing into the motor when the voltage-based flux-weakening control method is applied. In addition, problems caused by voltage errors were described using theoretical approaches and simulations. A method to resolve such problems was proposed, and its effect was verified through simulations and empirical experiments.

This research work is structured in different sections. Section 2 details the algorithm for basic voltage weak flux control. Moreover, the voltage error of conventional voltage flux-weakening control will be explained theoretically. Additionally, how the current changes due to a voltage error is explained. Section 3 describes the algorithm of the proposed voltage flux-weakening control. The design process of the proposed voltage flux-weakening control is explained and the effect is analyzed through simulation. In Section 4, the experimental results are verified and analyzed to validate the effectiveness of the proposed voltage flux-weakening control. Finally, Section 5 concludes the paper.

2. Analysis of the Application of Voltage-Based Flux-Weakening Control and Offset Voltage PWM

2.1. Application of Voltage-Based Flux-Weakening Control and Offset Voltage PWM

At present, vector control is mainly used to control motors. Vector control is a method to convert the three-phase voltage and current that change over time into time-invariant voltage and current components and control each component, which enables precise speed control as instantaneous motor speed control is possible.

Figure 1 shows a block diagram of the control using the voltage-based flux-weakening control and offset voltage PWM method among the vector controls used in synchronous motors. Vector controls measure the three-phase current flowing into the synchronous motor and convert it into d-axis (flux component) and q-axis (torque component) current components using the DQ transform. The converted current components create an error between the d-axis current reference and the q-axis current reference required for the synchronous motor to reach the target speed, and the amount of voltage is manipulated through the PI controller to control the speed of the synchronous motor. The performance variation is observed in the area where the motor is operated at high speed, depending on the algorithm applied to the flux-weakening control block and the PWM occurrence block.

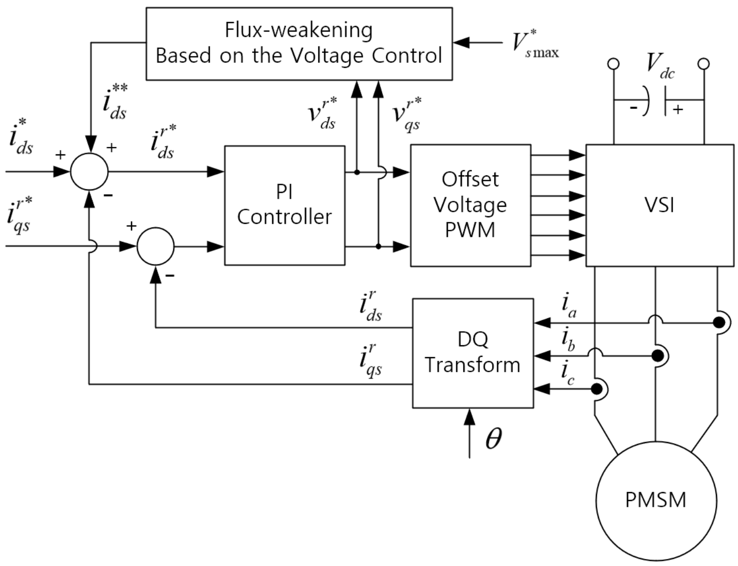

Figure 1. Block diagram of typical voltage-based flux-weakening control.

In this study, the voltage-based flux-weakening control and offset voltage PWM methods were simultaneously applied to maximize the magnitude of the voltage applied to the motor without being affected by the motor parameters.

When these two methods are applied simultaneously, the algorithm design is more straightforward than that of the flux-weakening control method using space vector PWM (SVPWM) and motor parameters. Thus, it provides the advantage of shortening the time to control, and the voltage can be controlled even in a particular overmodulation area.

However, when the general voltage-based flux-weakening control method and the offset voltage PWM method are simultaneously applied, an error may occur between the voltage applied to the motor in the overmodulation area and the predicted voltage used for the flux-weakening control. Owing to this error, the amount of current flowing through the motor can increase, leading to increased related losses.

2.2. Analysis of Command Voltage Following the Application of Offset Voltage PWM

The general voltage-based flux-weakening control uses the voltage value (v_s^*) calculated using v_{ds}^{r*} and v_{qs}^{r*}, which are the control inputs of the current PI controller. When voltage-based flux-weakening control and SVPWM are used in combination, there is no error between v_s^* and the actual voltage applied to the motor.

However, in the case of methods that use triangular signals as carrier signals, such as sinusoidal PWM (SPWM) and offset PWM, errors may occur between v_s^* and the voltage applied to the motor.

Figure 2 shows a block diagram of the detailed control of the offset PWM. In Figure 2, it can be seen that v_{ds}^{r*} and v_{qs}^{r*}, which are the control inputs of the current PI controller, are changed from two-phase voltage commands to three-phase voltage commands (v_a^*, v_b^*, v_c^*) through the inverse DQ transform. These are in turn converted into voltage commands (v_{sa}^*, v_{sb}^*, v_{sc}^*) injected with signals in the form of three harmonic waves through the reference generator, which can increase the maximum amplitude of the fundamental wave voltage applied to the motor. Thereafter, the voltage commands are converted into the final voltage commands (v_{la}^*, v_{lb}^*, v_{lc}^*) through the limiter that limits the voltage commands so as to not exceed the maximum amplitude of the carrier waves. Figure 3 shows the waveforms converted by the voltage command generated during this process.

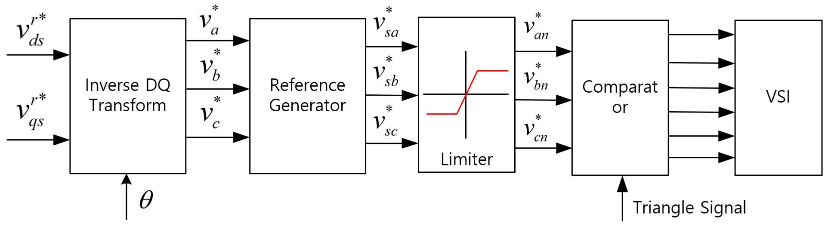

Figure 2. Block diagram of detailed control of offset PWM.

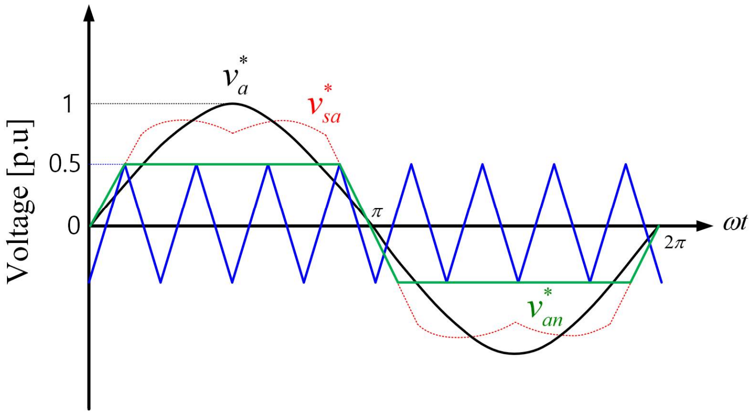

Figure 3. Graphs for voltage commands in the event of overmodulation.

Figure 3 shows the graphs for various voltage commands in the overmodulation area, where the magnitudes of the voltage commands were outside the area where they could be linearly controlled. Here, the maximum magnitudes of v_a^*, v_b^*, and v_c^* were set to 1 (p.u), and this was normalized to be the same as V_{dc}. When the motor is controlled using a general two-level three-phase voltage source inverter (VSI), the maximum magnitude of the triangular waves used in the comparator is expressed as $V_{dc}/2$.

Figure 4 shows the changes in v_{sn}^* when v_s^* is changed from 0 (p.u) to 1.0 (p.u) in the environment where the offset voltage PWM shown in Figure 2 is applied. In Figure 2, it can be seen that the magnitude of the fundamental wave increases linearly without any difference from v_{sn}^* when v_s^{r*} is not larger than approximately 0.5774 (p.u). This area is referred to as a "linear modulation area".

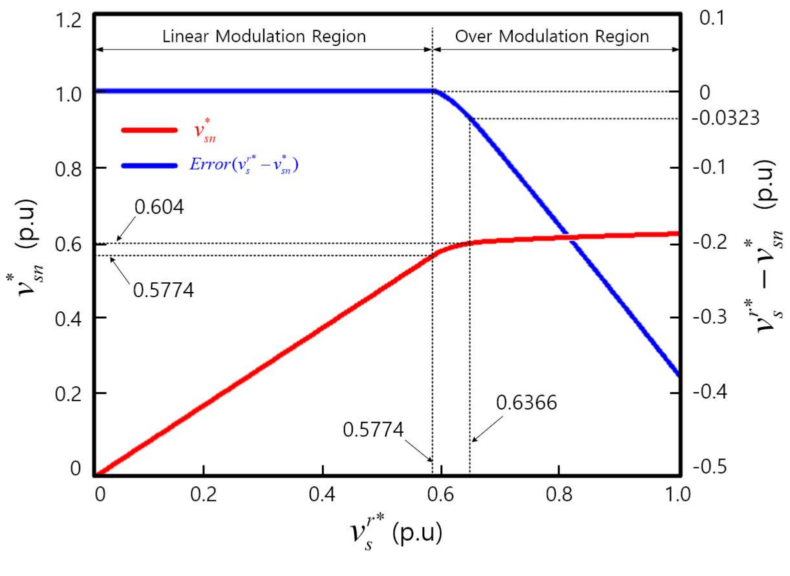

Figure 4. Graph representing the changes in v_{sn}^* with respect to command voltage v_s^{r*}.

The difference between v_s^{r*} and v_{sn}^* occurs when v_s^{r*} is approximately 0.5774 (p.u) or higher, and it can be seen that the difference increases as v_s^{r*} increases. The area where the magnitude of the fundamental waves increases nonlinearly is called an "overmodulation area". When overmodulation occurs, the maximum magnitude of v_{sa}^* is limited by the limiter, as shown in Figure 3, and as v_s^{r*} increases, v_{an}^* is converted into a trapezoidal shape [30].

Because the maximum magnitude of the fundamental waves generated using a perfect square wave is approximately 0.6366 times [31] of V_{dc}, it can be seen that when v_s^{r*} is applied as 0.6366 (p.u), v_{sn}^* is approximately 0.604 (p.u). In this case, the difference between the two voltage commands is approximately -0.0323 (p.u). When v_s^{r*} is applied as 0.604 (p.u), it can be observed that v_{sn}^* is approximately 0.594 (p.u), and the error, in this case, is estimated to be approximately -0.0323 (p.u). Hence, the use of v_s^{r*} in voltage-based flux-weakening control causes an error with respect to the actual voltage applied to the motor.

2.3. Analysis of Current Changes According to Voltage Error

If the voltage command converted into a trapezoidal shape is not considered, an error occurs between the voltage applied to the motor and the calculated voltage used for voltage-based flux-weakening control. This results in a voltage different from the intended voltage being applied to the motor, leading to a higher current flow than needed to generate torque, as shown in Figure 4. A theoretical approach should be used to examine changes in the amount of currents according to the voltage error. First, the equations of the limiting conditions for current and voltage are as follows [20]:

$$v_{qs}^{r\,2} + v_{qds}^{r\,2} \leq V_{smax}{}^2 \tag{1}$$

$$i_{qs}^{r\,2} + i_{ds}^{r\,2} \leq I_{smax}{}^2 \tag{2}$$

where i_{ds}^r and i_{qs}^r are d-axis component of stator current and q-axis component of stator current in the rotor reference frame, respectively.

Equations (1) and (2) represent the voltage-limiting condition and current-limiting condition, respectively. Equation (1) indicates that the magnitude of the command voltage generated by the PI controller is limited such that it does not exceed the circle whose radius is V_{smax}. Equation (2) is the current-limiting condition wherein the magnitude of the current applied to the motor is limited such that it does not exceed the circle with a radius of I_{smax}. The torque of the PMSM during vector control can be expressed as follows [32]:

$$T_e = \frac{3}{2} \cdot \frac{P}{2} \cdot \left\{ \left(L_d - L_q \right) i_{ds}^r i_{qs}^r + \lambda_f i_{qs}^r \right\} \tag{3}$$

where L_d and L_q are the direct axis and the intersecting axis inductance, respectively. λ_f is the rotor flux.

The surface-mounted permanent magnet synchronous motor (SPMSM) has the following characteristics due to the motor structure:

$$L_d = L_q \tag{4}$$

The torque Equation (3) can be transformed by considering Equation (4), as shown below:

$$T_e = \frac{3}{2} \cdot \frac{P}{2} \cdot \lambda_f i_{qs}^r \tag{5}$$

To calculate the amount of current generated owing to the error of the calculated voltage, Equation (5) can be transformed into an equation of i_{qs}^r as shown below:

$$i_{qs}^r = \frac{2}{3} \cdot \frac{2}{P} \cdot \frac{T_e}{\lambda_f} \tag{6}$$

where, if λ_f is used as a fixed variable that does not change, it can be observed that i_{qs}^r is changed only by T_e.

To determine the current required for T_e according to V_{smax} and motor speed, Equation (1) can be modified using the steady-state voltage equation for the PMSM as follows:

$$\left(\omega_r L_{qs} i_{qs}^{r*}\right)^2 + \left(\omega_r L_{ds} i_{ds}^{r*} + \omega_r \lambda_f\right)^2 \leq V_{smax}{}^2 \quad (7)$$

$$L_s = L_d = L_q \quad (8)$$

the above expression can be transformed into an expression for i_{ds}^r as follows:

$$i_{ds}^r \leq \frac{1}{L_s} \cdot \left\{ \sqrt{\left(\frac{V_{smax}}{\omega_r}\right)^2 - \left(L_s i_{qs}^r\right)^2} - \lambda_f \right\} \quad (9)$$

where if L_s and λ_f are assumed to be fixed variables, it can be seen that i_{ds}^r is affected by voltage and speed. Accordingly, a graph when Equations (1), (2), (7) and (9) are used, shown Figure 5.

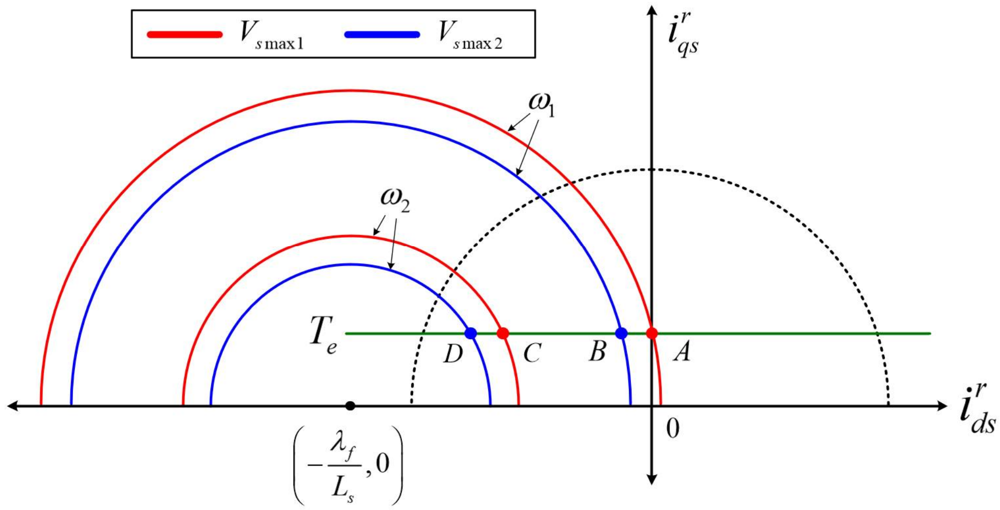

Figure 5. Voltage limiting circles according to changes in speed and voltage.

Figure 5 shows the voltage limiting circles according to the speed and voltage of the motor when a fixed T_e is applied to the SPMSM. Where V_{smax1} is greater than V_{smax2} and ω_2 is greater than ω_1. Point A is where the motor is controlled so as not to exceed V_{smax} and T_e, i_{qs}^{r*}, and the voltage limiting circle meet simultaneously. Point A is the speed at which the flux-weakening control starts. The current point is controlled such that the motor does not exceed V_{smax} owing to the current-limiting circle and the voltage-limiting circle. When the speed increases from ω_1 to ω_2, the current moves from point A to point C.

However, it can be seen that the sizes of the voltage- limiting circle are different according to V_{smax}, even when the speed is same, as shown in Equation (9) and Figure 5. Points A and B are on voltage limiting circles drawn at the same speed. However, the smaller the fundamental wave voltage applied to the motor, the smaller is the voltage limiting circle. This implies that the controlled current point may vary depending on the V_{smax} that can be applied to the motor. In the case where the current point of the ideal flux-weakening control is point A, if an error occurs in the calculated voltage such that a voltage smaller than the actual voltage is applied to the motor, the motor will be controlled with the current point at point B. This will increase the copper loss of the motor because more current is used at the same speed.

A similar result was obtained when the motor speed was increased to ω_2. Although the ideal current control point at ω_2 is point C, an error occurs in the calculated magnitude of V_{smax} such that the motor is controlled with the current point at point D. This also increases the copper loss because the current required to control the motor increases. Thus, the magnitudes of the current according to speed when the command voltages v_s^{e*} and v_{sn}^* are used can be illustrated, as shown in Figure 6.

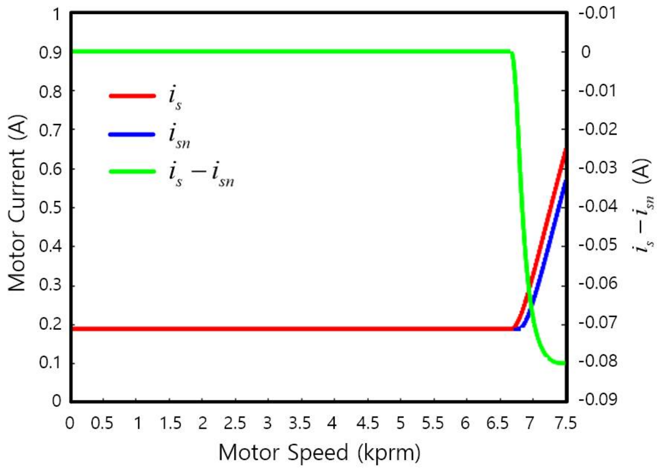

Figure 6. Graph of changes in the current according to V_{smax}.

Figure 6 shows a graph expressing the changes in the current of the motor according to the V_{smax} used. Equations (1)–(9) were used to express Figure 6, and the changes in current when a load of $T_e = 0.07$ (Nm) is constantly applied to a motor with parameters $\lambda_f = 0.0617$ (Wb) and $L_s = 110$ (mH) are expressed, where, i_s refers to the current when v_s^{r*} is used as the voltage of the flux-weakening control, and i_{sn} represents the current when v_{sn}^* is used as the calculated voltage.

In Figure 6, it can be seen that no error occurred between the two currents before the flux-weakening control began. However, differences between them occurred from the moment when the flux-weakening control was implemented. When the motor was controlled at 7500 (rpm), i_s was approximately 0.6517 (A), and i_{sn} was approximately 0.5719 (A). These are approximately 13.96(%) higher than the actual required current. Thus, it can be seen that the more the errors that occur in the calculated voltage used in the flux-weakening control, the higher the current applied to the motor.

Accordingly, a method to minimize the calculated voltage while performing voltage-based flux-weakening control is necessary.

3. Design and Verification of Improved Voltage-Based Flux-Weakening Control Algorithm

In this study, an improved indirect voltage-based flux-weakening control method, as shown in Figure 7, was proposed to overcome the aforementioned problems. This method reduces the voltage error applied to the PMSM in the overmodulation area by changing the voltage used in the voltage-based flux-weakening control.

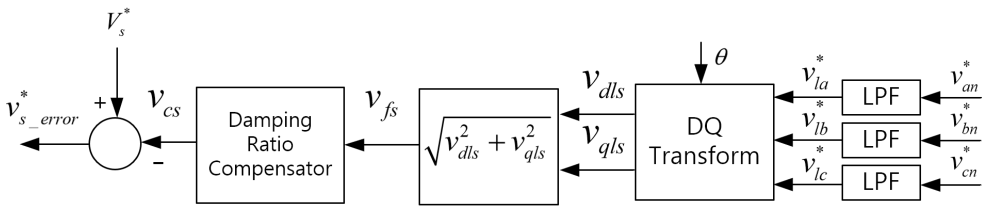

Figure 7. Block diagram of the improved indirect voltage-based flux-weakening control.

The improved indirect voltage-based flux-weakening control uses v_{an}^*, v_{bn}^*, and v_{cn}^*, as shown in Figure 5. When the voltage is calculated using only v_{an}^*, v_{bn}^*, and v_{cn}^*, the voltage of the DC component, including the AC component, is calculated considering the harmonics generated in the trapezoidal shape. This may act as an element that lowers the accuracy of the PI controller in the overmodulation area. Therefore, an additional algorithm is required. Accordingly, a low-pass filter and a damping ratio compensator may be configured to filter the harmonics generated in the trapezoidal shape.

3.1. Design of Low-Pass Filter

For v_{an}^*, v_{bn}^*, and v_{cn}^*, it is essential to minimize the harmonic component in one period. Accordingly, a digital low-pass filter (LPF) was designed to remove the harmonics of v_{an}^*, v_{bn}^*, and v_{cn}^* before performing the DQ transform. In this case, the LPF can be configured using a simple first-order system, and the noise and harmonics in the frequency band desired by the user can be attenuated using Equation (10) below.

$$H(s) = \frac{v_{lx}^*(s)}{v_{xn}^*(s)} = \frac{\omega_c}{s+\omega_c} \qquad (x = a, b, c) \tag{10}$$

where w_c represents the cut-off frequency, and the maximum angular speed at which the motor can be controlled can be set to w_c.

3.2. Design of Damping Ratio Compensator

If the LPF is used, the magnitude of the voltage in the harmonic area can be attenuated, as shown in Equation (10). However, the magnitude of the voltage in areas other than the harmonic area is also attenuated. If flux-weakening control is performed using the reduced voltage, errors occur when generating the voltage of the desired magnitude. Here, the rate at which the magnitude of the voltage decreases can be defined as the damping ratio, which can be expressed using Equation (11), where ω is the angular velocity of the motor.

$$|H(s)| = \frac{1}{\sqrt{\left(\frac{\omega}{\omega_c}\right)^2 + 1}} \tag{11}$$

$$v_{lx}^* = \frac{1}{\sqrt{\left(\frac{\omega}{\omega_c}\right)^2 + 1}} v_{xn}^* \qquad (x = a, b, c) \tag{12}$$

From Equation (10), it can be seen that the magnitude of the voltage (dB) decreases as the frequency increases. In the case of the frequency band of 500 (Hz), because the voltage is attenuated by approximately -3.01 (dB), v_{la}^* has a magnitude of voltage attenuated by approximately $\sqrt{2}$ times compared to v_{an}^*. To use the LPF, it is necessary to compensate for the magnitude of the attenuated voltage. The phase difference of the voltage calculated by the LPF is negligible as it is only the magnitude of the voltage used in the indirect voltage flux-weakening control.

The angular velocity of the motor was measured to perform vector control. Because the angular velocity of the rotor in a synchronous motor is the same as the velocity of the rotating magnetic field, the damping ratio compensation can be easily performed using the measured angular velocity. Accordingly, the magnitude of the attenuated voltage can be compensated by using the following equation:

$$v_{cs} = \sqrt{\left(\frac{\omega}{\omega_c}\right)^2 + 1} \cdot v_{fs} \tag{13}$$

3.3. Verification of the Effect of the Improved Voltage-Based Flux-Weakening Control through Simulation

Simulations were conducted to verify the effect of the proposed voltage-based flux-weakening control. The simulations were performed using a PSIM simulator, and the motor model of the SPMSM provided by the PSIM was used. The parameters used for the motor and inverter in the simulations are listed in Table 1, and the simulations were conducted when flux-weakening control was performed using v_s^{r*} and v_{sn}^*, respectively, where the average of every 10 measured data points was obtained to show the waveform.

Table 1. Summary of various parameters used in the simulations.

Device	Parameter	Unit	Value
Inverter	DC-LINK voltage	(V)	290
	Max current	(A)	3.82
	Switching frequency	(Hz)	20,000
Motor	Back EMP(Ke)	(Vpk/krpm)	49
	Number of poles	(P)	8
	Resistance	(Ω)	2.2
	Inductance	(H)	0.0109
	Inertia	$(\mathrm{oz}-\mathrm{in}-\mathrm{sec}^2)$	0.00439

Figure 8 shows the waveforms in the simulation results when the motor speed was increased to 7500 (rpm) using the inverter, as shown in Table 1, where V_{smax} was fixed at 0.604 (p.u). As shown in Figure 8a, when flux-weakening control was performed using v_s^*, the rotation speed of the motor reached the maximum command speed of 7500 (rpm) normally. When v_{sn}^* was used, the rotation speed of the motor reached the maximum command speed of 7500 (rpm) normally. Thus, it can be seen that there are no issues in the operation of the motor at speeds up to 7500 (rpm) in both cases.

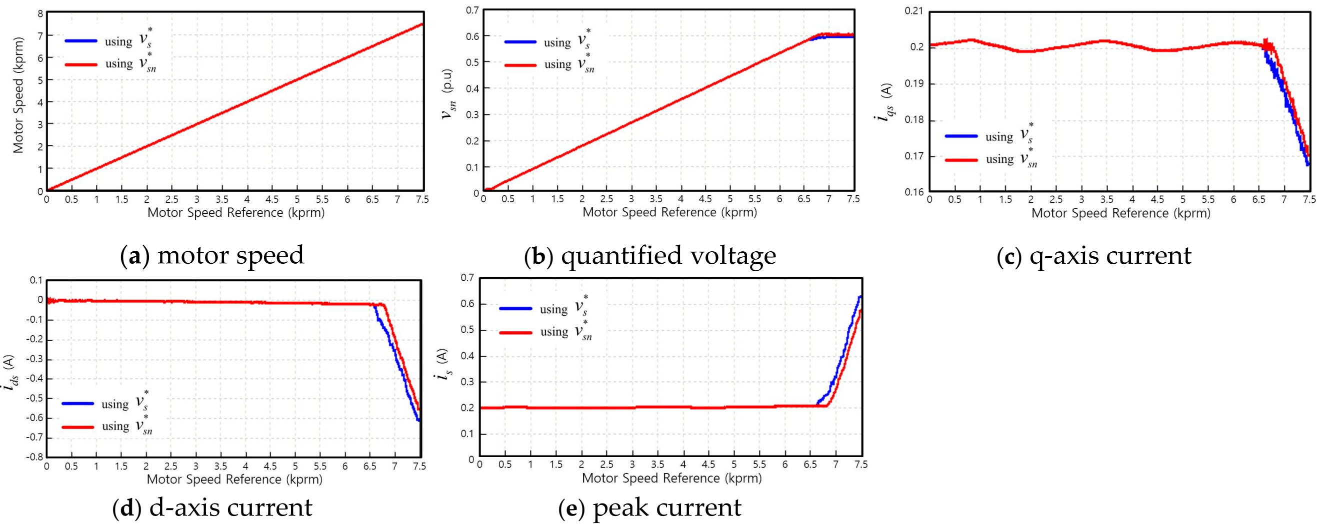

(**a**) motor speed (**b**) quantified voltage (**c**) q-axis current

(**d**) d-axis current (**e**) peak current

Figure 8. Simulation results according to changes in motor speed command.

From the results when flux-weakening control was performed using v_s^*, shown in Figure 8b, it can be seen that when the rotation speed of the motor reached 7500 (rpm), v_{sn} was measured to be approximately 0.597 (p.u). When the motor was controlled using v_{sn}^*, v_{sn} at 7500 (rpm) was measured to be approximately 0.605 (p.u). These results were consistent with the results shown in Figure 4, and it was confirmed that the presented error between the voltages could occur, and the error was measured to be approximately 0.08 (p.u).

From Figure 8c, it can be seen that as SPMSM was used in the simulations, an average current of approximately 0.2 (A) was injected in both methods until flux-weakening control began. However, as the flux-weakening control began, i_{qs} decreased slightly.

The voltage error shown in Figure 8c dominates the effect of i_{ds}. Figure 8d shows that when flux-weakening control was performed using v_s^*, flux-weakening control began from approximately 6570 (rpm), and i_{ds} began to be injected thereafter and was measured to be approximately -0.688 (A) when the rotation speed reached 7500 (rpm). When v_{sn}^* was used, it can be seen that the flux-weakening control began from approximately 6800 (rpm), and i_{ds} began to be injected thereafter and was measured to be approximately -0.543 (A) when the rotation speed reached 7500 (rpm). This current is approximately 0.189 (A) smaller than when flux-weakening control was performed using v_s^*. It can be concluded that this is the best result that can be obtained by minimizing the voltage error. As a result of the simulations described above, it can be seen that the possibility of errors in the voltage presented in Section 2, and the resultant change in the amount of the current appear.

4. Experimental Results and Discussion

4.1. Construction of Experimental Environment and Design of Conditions

To verify the actual effect of the improved voltage-based flux-weakening control, a 400 (W) class PMSM was used. The PMSM used in the experiment was the HVPMSMMTR model of Texas Instruments, and the motor drive inverter module used in the experiment was the TMDSHVMTRINSPIN model. The parameters of the inverter, controller, and motor used in the experiment were the same as those listed in Table 1.

4.2. Comparison and Analysis of Experimental Results

Figure 9 shows the results of the measurement of the current and pole voltage of one phase when the general voltage-based flux-weakening control and the improved voltage-based flux-weakening control were used, respectively.

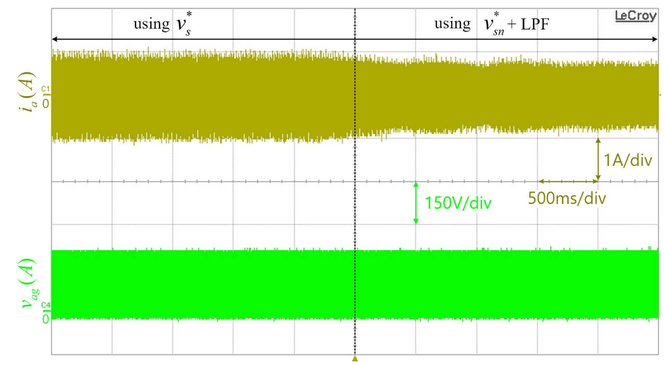

(**a**) variable voltage source

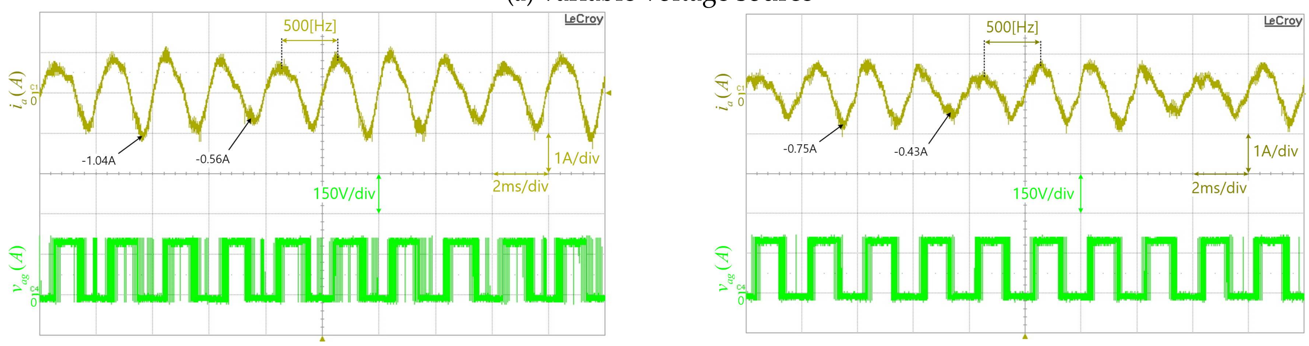

(**b**) using v_s^* (**c**) using v_{sn}^*

Figure 9. Waveforms in the experiment results when motor speed is 7500 (rpm).

Figure 9a shows the waveform measured while the motor rotated at 7500 (rpm) and flux-weakening control was carried out using v_{sn}^* before 2.5 (s) and using v_{sn}^* after 2.5 (s). Observing the a-phase current measured in this case, it can be seen that the maximum magnitude of the current became smaller when v_{sn}^* was used than when v_s^* was used.

As shown in Figure 9b, which presents the enlarged waveform when v_s^* was used, the frequency of the a-phase current was measured to be approximately 500 (Hz). As the number of poles of the motor used in the experiment was 8, it can be seen that the frequency that must be used when the measured current is 7500 (rpm) is being injected normally. Observing the a-phase current, it can be seen that the largest current among the peak currents was measured to be approximately -1.04 (A), and the smallest current among the peak currents was measured to be approximately -0.56 (A).

As shown in Figure 9c, which presents the enlarged waveform when v_{sn}^* was used, the frequency of the a-phase current is also measured to be approximately 500 (Hz), indicating that a current appropriate for 7500 (rpm) is injected. On reviewing the measured currents, it can be seen that the largest current among the peak currents was measured to be approximately -0.75 (A), and the smallest current among the peak currents was measured to be approximately -0.43 (A). On reviewing the a-phase pole voltage, it can be seen that it is controlled to be closer to square waves than the pole voltage in Figure 9b.

That is, the magnitude of the current became smaller when v_{sn}^* was used than when flux-weakening control was carried out using v_s^* at the same frequency of 500 (Hz). This indicates that the proposed voltage-based flux-weakening control method can alleviate the voltage error problem of the general method.

To compare and analyze the experimental data, the motor data were extracted using the conditions listed in Table 2. In addition, all the data extracted by the speed command were averaged and are shown in Figure 10.

Table 2. Experimental environment conditions.

Parameters	Unit	Value
Total Experiment Time	(min)	12.5
Maximum Motor Speed	(rpm)	7500
Motor Speed Variable Width	(rpm)	100
Variable Time Width	(s)	10
Reference Voltage Max (V_{smax})	(V)	0.604

Figure 10 shows a graph depicting the motor rotation speeds i_{ds}, i_{qs}, i_s, and v_{sn} according to the voltage used for flux-weakening control carried out after setting V_{smax} to 0.604 (p.u). In Figure 10a, it can be seen that when flux-weakening control was carried out using v_s^*, the rotational speed of the motor normally reached the maximum command speed of 7500 (rpm). Experiments were conducted when v_{sn}^* was used, and according to the results, the motor's rotational speed normally reached the maximum command speed of 7500 (rpm). That is, in both cases, control is possible at the desired command speed.

As shown in Figure 10b, according to the results when flux-weakening control was performed using v_s^*, v_{sn} was measured to be approximately 0.59 (p.u) when the rotational speed of the motor reached 7500 (rpm). When the motor was controlled using v_{sn}^*, v_{sn} was measured to be approximately 0.604 (p.u) when the command speed of the motor reached 7500 (rpm). These results were almost identical to the results shown in Figure 7, indicating that the presented error occurred between the voltages.

In the case where flux-weakening control was performed using v_s^*, Figure 10c shows that the flux-weakening control began from approximately 6600 (rpm), and i_{ds} began to be injected thereafter and was measured to be approximately -0.644 (A) when the rotational speed of the motor reached 7500 (rpm). When v_{sn}^* was used, it can be seen that the flux-weakening control began from approximately 6800 (rpm), and i_{ds} began to be injected thereafter and was measured to be approximately -0.454 (A) when the rotational speed of the motor reached 7500 (rpm). In this case, a smaller current by approximately 0.189 (A) was used than when flux-weakening control was performed using v_s^*.

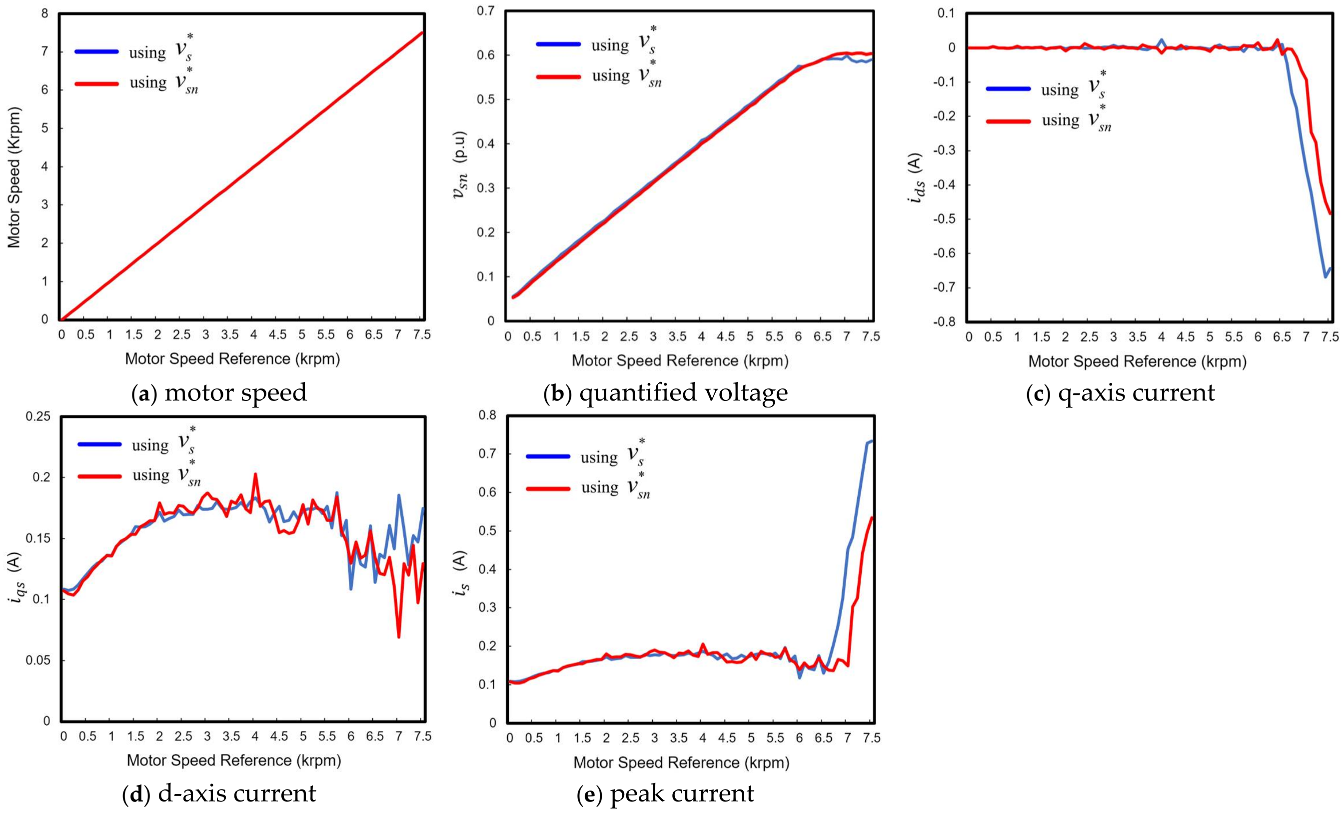

(**a**) motor speed (**b**) quantified voltage (**c**) q-axis current

(**d**) d-axis current (**e**) peak current

Figure 10. Experiment results according to changes in motor speed command.

As shown in Figure 10d, i_{qs} was similarly injected into the motor. At the beginning of the motor operation, approximately 0.108 (A) of i_{qs} was injected, but as the speed increased, it can be seen that up to approximately 0.18 (A) of i_{qs} was injected owing to the moment of inertia of the motor. As the SPMSM was used, the current point trajectory required for T_e was in the form of a straight line, as shown in Figure 5, and the amount of change in i_{qs} was small.

As shown in Figure 10c, when flux-weakening control was performed using v_s^*, flux-weakening control began from approximately 6600 (rpm), and i_{ds} began to be injected thereafter and was measured to be approximately -0.644 (A) when the rotational speed of the motor reached 7500 (rpm). As a result of performing flux-weakening control using only v_{sn}^*, i_{ds} was changed from approximately 6700 (rpm) but was not reduced further than approximately -0.06 (A). When v_{sn}^* and LPF were used simultaneously, it can be seen that the flux-weakening control began from approximately 6800 (rpm), and i_{ds} began to be injected thereafter and was measured to be approximately -0.454 (A) when the rotational speed of the motor reached 7500 (rpm). This indicates that the motor was controlled using a current that is approximately 0.189 (A) smaller than that when flux-weakening control was performed using v_s^*, and the voltage error was minimized.

As shown in Figure 10d, when flux-weakening control was performed using v_s^*, i_s was measured to be approximately -0.733 (A) when the motor's rotational speed reached 7500 (rpm). When v_{sn}^* and LPF were used simultaneously, it can be seen that the flux-weakening control began from approximately 6800 (rpm), and i_{ds} began to be injected thereafter and was measured to be approximately 0.534 (A) when the motor's rotational speed reached 7500 (rpm). This indicates that the motor was controlled using a current that is approximately 0.2 (A) smaller than that when flux-weakening control was performed using v_s^*, and the voltage error could be minimized.

When the results in Figure 10 are synthesized, it can be seen that when the motor speed is controlled using v_s^*, high-speed operation is normally performed through flux-weakening control. However, it can be seen that a larger amount of i_{ds} than the i_{ds} appropriate for the speed command is applied to the motor because of the error between the actual voltage applied to the motor and the calculated voltage.

When the motor speed is controlled using v_{sn}^*, high-speed operation is normally performed through flux-weakening control. In addition, the error between the actual voltage applied to the motor and the calculated voltage is minimized so that only the i_{ds} appropriate for the speed command can be used to control the motor.

As the theoretical approaches, simulations, and experimental results were consistent, it could be inferred that the proposed voltage-based flux-weakening control is applicable and that the voltage error can be minimized.

5. Conclusions

This paper presents an improved voltage-based flux-weakening control method to enhance the performance of synchronous motors using a voltage-based flux-weakening control. This method mitigates the errors occurring between the voltage command used in previous methods and the voltage flowing into the motor. The possibility that errors may occur between the voltage command and the voltage flowing into the motor in the previously used method was considered, and the problems were analyzed through a theoretical approach and simulations.

As a result of theoretically approaching the error that occurred, when the magnitude of the voltage in the flux-weakening control region was out of the linear region, the voltage command was transformed into a trapezoidal shape. The magnitude of the fundamental wave in the transformed trapezoidal shape was smaller than the magnitude of the fundamental wave of the voltage command, so the magnitude of the voltage applied to the motor was reduced. Accordingly, it was confirmed that the size of the voltage limit circle was reduced, and the required current was increased under the same torque condition.

According to the comparison and analysis results of the effects of the general indirect voltage method and the proposed method through experiments, when the improved voltage flux-weakening control was applied to the PMSM, the voltage errors were reduced by approximately 2.16(%) compared to the general method. Accordingly, energy efficiency was improved by reducing the current used in the field-weakening control region by up to 27.17(%) under the same torque condition. The proposed method can be applied to motors using a voltage-based flux-weakening control to increase the energy efficiency in the control area. It can be used for various feedback and feed-forward control methods using voltage commands. In future research, we plan to continuously compare and analyze the effects of applying the results of this paper to various studies using voltage commands.

Author Contributions: Conceptualization, H.-J.L. and J.-G.S.; methodology, H.-J.L. and J.-G.S.; software, H.-J.L.; validation, J.-G.S.; formal analysis, H.-J.L.; writing—original draft preparation, H.-J.L.; writing—review and editing, H.-J.L. and J.-G.S.; supervision, J.-G.S. All authors have read and agreed to the published version of the manuscript.

Funding: This work was supported by the Korea Institute of Energy Technology Evaluation and Planning (KETEP) and the Ministry of Trade, Industry and Energy (MOTIE) of the Republic of Korea (no. 20214000000060) and was supported by the Gachon University research fund of 2021 (GCU-202004440001).

Conflicts of Interest: The authors declare no conflict of interest.

References

1. 2050 Carbon Neutral Strategy of the Republic of Korea towards a Sustainable and Green Society. 2020. Available online: https://unfccc.int/sites/default/files/resource/LTS1_RKorea.pdf (accessed on 4 November 2021).
2. SDSN. *Zero Carbon Action Plan*; Sustainable Development Solutions Network (SDSN): New York, NY, USA, 2020.
3. Hasoun, M.; Afia, A.E.L.; Chikh, K.; Khafallah, M.; Benkirane, K. A PWM Strategy for Dual Three-Phase PMSM Using 12-Sector Vector Space Decomposition for Electric Ship Propulsion. In Proceedings of the 2018 19th IEEE Mediterranean Electrotechnical Conference, Marrakech, Morocco, 2–7 May 2018; pp. 243–248. [CrossRef]
4. Hasoun, M.; Afia, A.E.l.; Chikh, K.; Khafallah, M. Field Oriented Control of Dual Three-Phase PMSM Based Vector Space Decomposition for Electric Ship Propulsion. In Proceedings of the 2019 International Conference of Computer Science and Renewable Energies, Agadir, Morocco, 22–24 July 2019; pp. 1–6. [CrossRef]
5. Sieklucki, G. Optimization of Powertrain in EV. *Energies* **2021**, *14*, 725. [CrossRef]
6. Hu, X.; Martinez, C.M.; Yang, Y. Charging, power management, and battery degradation mitigation in plug-in hybrid electric vehicles: A unified cost-optimal approach. *Mech. Syst. Signal Process.* **2017**, *87*, 4–16. [CrossRef]
7. Yao, M.; Qin, D.; Zhou, X.; Zhan, S.; Zeng, Y. Integrated optimal control of transmission ratio and power split ratio for a CVT-based plug-in hybrid electric vehicle. *Mech. Mach. Theory* **2019**, *136*, 52–71. [CrossRef]
8. Pillay, P.; Knshnan, R. Modeling of Permanent Magnet Motor Drives. *IEEE Trans. Ind. Electron.* **2008**, *55*, 2246–2257. [CrossRef]
9. Fang, S.; Liu, H.; Wang, H.; Yang, H.; Lin, H. High Power Density PMSM with Lightweight Structure and High-Performance Soft Magnetic Alloy Core. *IEEE Trans. Appl. Supercond.* **2019**, *29*, 0602805. [CrossRef]
10. Tong, W.; Dai, S.; Wu, S.; Tang, R. Performance Comparison between an Amorphous Metal PMSM and a Silicon Steel PMSM. *IEEE Trans. Magn.* **2019**, *55*, 8102705. [CrossRef]
11. Jeong, M.T.; Lee, K.B.; Pyo, H.Y.; Nam, D.W.; Kim, W.H. A Study on the Shape of the Rotor to Improve the Performance of the Spoke-Type Permanent Magnet Synchronous Motor. *Energies* **2021**, *14*, 3785. [CrossRef]
12. Fan, W.J.; Zhu, X.Y.; Quan, L.; Wu, W.Y.; Xu, L.; Liu, Y.F. Flux-Weakening Capability Enhancement Design and Optimization of a Controllable Leakage Flux Multilayer Barrier PM Motor. *Trans. Ind. Electron.* **2021**, *68*, 7814–7825. [CrossRef]
13. Gerada, D.; Mebarki, A.; Brown, N.L.; Gerada, C.; Cavagnino, A.; Boglietti, A. High-speed electrical machines: Technologies, trends, and developments. *IEEE Trans. Ind. Electron.* **2014**, *61*, 2946–2959. [CrossRef]
14. Ahn, J.H.; Han, C.; Kim, C.W.; Choi, J.Y. Rotor design of high-speed permanent magnet synchronous motors considering rotor magnet and sleeve materials. *IEEE Trans. Appl. Supercond.* **2018**, *28*, 5201504. [CrossRef]
15. Chen, Y.Z.; Huang, X.Y.; Wang, J.; Niu, F.; Zhang, J.; Fang, Y.T.; Wu, L.J. Improved Flux-Weakening Control of IPMSMs Based on Torque Feedforward Technique. *IEEE Trans. Power. Electron.* **2018**, *33*, 10970–10978. [CrossRef]
16. Deng, T.; Su, Z.H.; Li, J.Y.; Tang, P.; Chen, X.; Liu, P. Advanced Angle Field Weakening Control Strategy of Permanent Magnet Synchronous Motor. *IEEE Trans. Veh. Technol.* **2019**, *68*, 3424–3435. [CrossRef]
17. Zhang, X.A.; Foo, G.H.B.; Rahman, M.F. A Robust Field-Weakening Approach for Direct Torque and Flux Controlled Reluctance Synchronous Motors with Extended Constant Power Speed Region. *IEEE Trans. Ind. Electron.* **2020**, *67*, 1813–1823. [CrossRef]
18. Manzolini, V.; Rù, D.D.; Bolognani, S. An Effective Flux Weakening Control of a SyRM Drive Including MTPV Operation. *IEEE Trans. Ind. Appl.* **2019**, *55*, 2700–2709. [CrossRef]
19. Xu, X.; Novotny, D.W. Selecting the flux reference for induction machine drives in the field weakening region. *IEEE Trans. Ind. Appl.* **1992**, *28*, 1353–1358. [CrossRef]
20. Kim, S.H.; Sul, S.K. Maximum Torque Control of an Induction Machine in the Field Weakening Region. *IEEE Trans. Ind. Appl.* **1995**, *31*, 787–794. [CrossRef]
21. Ye, M.T.; Shi, T.N.; Wang, H.M.; Li, X.M.; Xia, C.L. Sensorless-MTPA Control of Permanent Magnet Synchronous Motor Based on an Adaptive Sliding Mode Observer. *Energies* **2019**, *12*, 3773. [CrossRef]
22. Wang, M.Z.; Sun, D.; Zheng, Z.H.; Nian, H. A Novel Lookup Table Based Direct Torque Control for OW-PMSM Drives. *IEEE Trans. Ind. Electron.* **2021**, *68*, 10316–10320. [CrossRef]
23. Lee, D.Y.; Lee, J.H. Compensation of Interpolation Error for Look-Up Table-Based PMSM Control Method in Maximum Power Control. *Energies* **2021**, *14*, 5526. [CrossRef]
24. Lee, D.Y.; Lee, J.H. Low Cost Simple Look-Up Table-Based PMSM Drive Considering DC-Link Voltage Variation. *Energies* **2020**, *13*, 3904. [CrossRef]
25. Jacob, J.; Bottesi, O.; Calligaro, S.; Petrella, R. Design Criteria for Flux-Weakening Control Bandwidth and Voltage Margin in IPMSM Drives Considering Transient Conditions. *IEEE Trans. Ind. Appl.* **2021**, *57*, 4884–4900. [CrossRef]
26. Miguel-Espinar, C.; Heredero-Peris, D.; Gross, G.; Llonch-Masachs, M.; Montesinos-Miracle, D. Maximum Torque per Voltage Flux-Weakening Strategy with Speed Limiter for PMSM Drives. *IEEE Trans. Ind. Electron.* **2021**, *68*, 9254–9264. [CrossRef]
27. Sepulchre, L.; Fadel, M.; Pietrzak-David, M.; Porte, G. MTPV Flux-Weakening Strategy for PMSM High Speed Drive. *IEEE Trans. Ind. Appl.* **2018**, *54*, 6081–6089. [CrossRef]
28. Dong, Z.; Yu, Y.; Li, W.; Wang, B.; Xu, D. Flux-Weakening Control for Induction Motor in Voltage Extension Region: Torque Analysis and Dynamic Performance Improvement. *IEEE Trans. Ind. Electron.* **2018**, *65*, 3740–3751. [CrossRef]
29. Kim, S.H.; Sul, S.K. Voltage Control Strategy for Maximum Torque Operation of an Induction Machine in the Field-Weakening Region. *IEEE Trans. Ind. Electron.* **1997**, *44*, 512–518. [CrossRef]

30. Sotorrio-Ruiz, P.J.; Sanchez-Pacheco1, F.J.; Perez-Hidalgo, F.M.; Heredia-Larrubia, J.R. Modulation of a trapezoidal signal: Improving signal quality and reducing costs in power inverters. *IET Power Electron.* **2017**, *10*, 568–576. [CrossRef]
31. Ogbuka, C.U.; Nwosu, C.M.; Odo, M.C. Fourier Analysis of Six Step Inverter Controlled Three Phase Induction Motor Drive. *NIEEE J. Res. Innov. Technol.* **2018**, *1*, 19–23.
32. Ranjan, S.; Sreejeth, M. Minimisation of Ripples in Torque of Hysteresis Current Controlled PMSM using PI-RES Controller. In Proceedings of the 2021 2nd International Conference for Emerging Technology, Belagavi, India, 21–23 May 2021; pp. 1–6. [CrossRef]